



# Detachment of a Rigid Flat Punch from a Viscoelastic Material

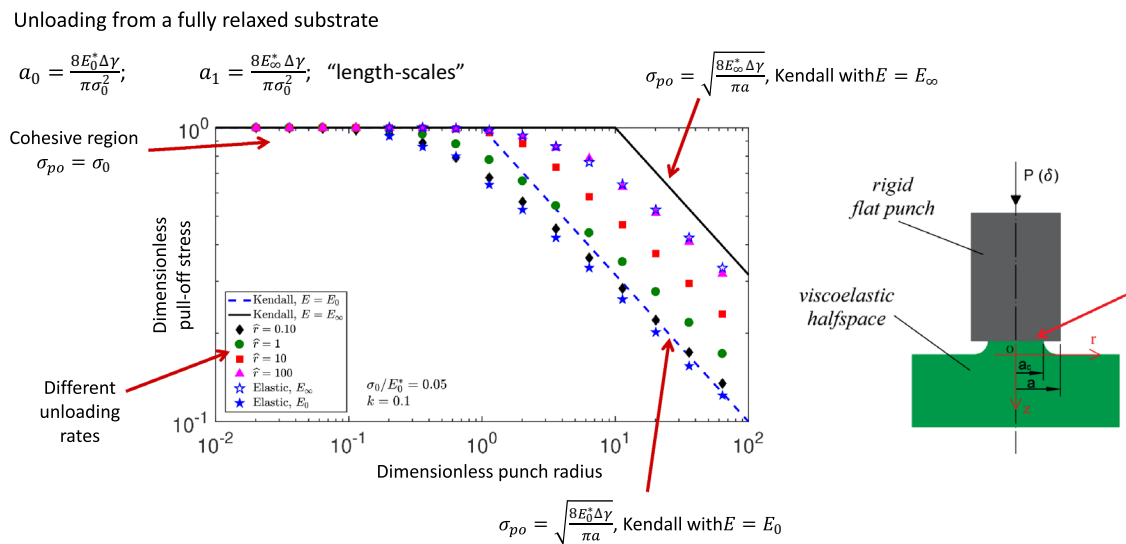
Antonio Papangelo<sup>1,2</sup> · Michele Ciavarella<sup>1,2</sup>

Received: 24 November 2022 / Accepted: 14 March 2023 / Published online: 1 April 2023  
 © The Author(s) 2023, corrected publication 2023

## Abstract

We show that the detachment of a flat punch from a viscoelastic substrate has a relatively simple behaviour, framed between the Kendall's elastic solution at the relaxed modulus and at the instantaneous modulus, and the cohesive strength limit. We find hardly any dependence of the pull-off force on the details of the loading process, including maximum indentation at preload and loading rate, resulting much simpler than the case of a spherical punch. Pull-off force peaks at the highest speeds of unloading, when energy dissipation is negligible, which seems to be in contrast with what suggested by the theories originated by de Gennes of viscoelastic semi-infinite crack propagation which associated enhanced work of adhesion to dissipation.

## Graphical abstract



**Keywords** Viscoelasticity · Crack propagation · Cohesive models · Energy balance

✉ Michele Ciavarella  
 mciava@poliba.it

Antonio Papangelo  
 antonio.papangelo@poliba.it

<sup>1</sup> Department of Mechanics Mathematics and Management, Politecnico di Bari, via Orabona 4, Bari 70125, Italy

<sup>2</sup> Department of Mechanical Engineering, Hamburg University of Technology, Am Schwarzenberg-Campus 1, Hamburg 21073, Germany

## 1 Introduction

Over the last two decades, there has been a tremendous interest in soft adhesive interfaces in various areas of technology, and in particular, those based on the van der Waals forces, which have been largely inspired by nature. Bio-inspired technologies are a growing area in robotics and grasping/pick-and-place manipulation [1, 2], since they show several

advantages such as high adhesive strength competitive to suction devices, more sustainable technology, recyclability, absence of residues [3], adaptability [4] and less energy consumption with respect to classical solutions [5]. Examples of application in several emerging technologies are described in [6], in robotics [7, 8] and in pick-and-place manipulation, also in space [9, 10].

In hard materials, van der Waals adhesive forces are destroyed very easily by roughness, and Dahlquist postulated, based on experiments on pressure sensitive adhesives (PSA), that the elastic modulus for them should be less than about 0.3 MPa [11] for sufficient adhesion. Soft materials are thus widely adopted in engineering, and those are often viscoelastic, which is pushing the research in the area of viscoelastic crack growth in soft media like polymers or biological materials [12, 13]. Early extensive measurements mostly with peeling setups [14–19] found that the peeling load increased very significantly with peeling speed. Since work of adhesion is equal to load for an elastic peeling problem according to the Rivlin classical solution for the typical 90° peeling conditions [20] for which the force per unit length of elastic peeling is exactly the work of adhesion, measuring the force in a viscoelastic tape generated the concept of “apparent work of adhesion  $\Delta\gamma$ ” obtained as the product of the adiabatic value  $\Delta\gamma_0$  and a function of crack velocity  $V$  of the contact/crack line and temperature, often in the form of a power law

$$\frac{\Delta\gamma(V)}{\Delta\gamma_0} = 1 + \left(\frac{V}{V_{\text{ref}}}\right)^n, \quad (1)$$

where  $V_{\text{ref}} = (ka_T^n)^{-1}$  and  $k, n$  are constants with  $0 < n < 1$  and  $a_T$  is the Williams–Landel–Ferry (WLF) shift factor to translate viscoelastic modulus results at various temperatures  $T$  [21]. The Williams–Landel–Ferry equation (or WLF equation) permits time-temperature superposition by the following formula

$$\log_{10} a_T = -\frac{C_1(T - T_r)}{C_2 + (T - T_r)}, \quad (2)$$

where  $T$  is the temperature,  $T_r$  is a reference temperature chosen to construct the compliance master curve and  $C_1, C_2$  are empirical constants adjusted to fit the values of the superposition parameter  $a_T$ . In other words, measurements at different temperatures permit to obtain a wide range of frequency estimate of the complex modulus of viscoelastic material which would otherwise not be obtained in a single experiment with a restricted range of frequencies via

$$E(\omega, T) = E(a_T\omega, T_r). \quad (3)$$

Equation (1) is known as the Gent–Schultz “empirical law” [15], and is widely adopted even to different

geometries, although the constants may depend on geometry (in peeling itself, there is certainly an effect of the angle of peeling). Notice that in this form there is no indication about the maximum enhancement, although the connection to the WLF factor indicates a link with elastic modulus whose increase has clear limits. However, peeling experiments such as Gent and Petrich [16] showed a maximum in peel force followed by a decrease in an unstable regime and stick–slip. It is remarkable that peeling experiments are still not entirely understood: in a peeling geometry of a viscoelastic tape it would seem that speed-dependence of the load of typical 90° angles would be precluded in a rate-independent cohesive stress model (see a detailed recent study in [22]) like the present model or the Knauss–Schapery or de Gennes–Persson–Brenner theories we are discussing in the present paper, yet it is clearly observed. The case of viscoelastic peeling seems to require rate-dependence in the cohesive (or the cut-off) stress.

From a more fundamental perspective, the need of Cohesive Zone Model (CZM) formulations to describe the crack propagation in viscoelastic media was evident in the 1970s [23–27]. Knauss–Schapery showed that when the stress field is well defined by an “applied” stress intensity factor  $K_A$ , the speed of propagation was defined by a generalized Irwin equation which for pure mode I reads

$$\Delta\gamma_0 = C(t_b)K_A^2, \quad (4)$$

where the linear viscoelastic creep compliance  $C(t)$  replaces the elastic compliance  $((1 - \nu^2)/E$  in plane strain,  $1/E$  in plane stress, where  $E$  is Young’s modulus and  $\nu$  is Poisson’s ratio) in the very similar Linear Elastic Fracture Mechanics (LEFM) critical equivalent condition, and  $t_b$  is an effective time of relaxation in the cohesive zone. This equation is valid for any geometry, provided the cohesive zone length  $b$  is small with respect to other length scales in the problem. In other words, in this model the “true” work of adhesion is rate-independent, and yet it results in load enhancement.

An alternative approach returns to the concept of the “apparent work of adhesion” and stems from the seminal work by de Gennes [28] who attributed it to dissipation possibly very far ahead from the crack tip in the so-called “liquid” zone—a concept which Persson and Brenner [29] elaborated in more quantitative terms, still for semi-infinite cracks. Despite the different approaches, both dissipation-based and CZM-based theories provide similar results for semi-infinite cracks and obtain the same maximum toughness enhancement [30]

$$\frac{\Delta\gamma(\infty)}{\Delta\gamma_0} = \frac{E_\infty}{E_0}, \quad (5)$$

being  $E_0$  and  $E_\infty$  the so-called relaxed and instantaneous modulus of the viscoelastic material, if we interpret as “apparent work of adhesion”

$$\Delta\gamma(V) = \frac{K_A^2}{E_0} \tag{6}$$

The question is less clear for any finite size body [31, 32], for which de Gennes postulated dissipation is restricted in space and so should reach a maximum and then decay with speed [28]. This was intended to perhaps explain the well-known Gent and Petrich [16] results for peeling experiments which we have mentioned. However, while in peeling experiments load and work of adhesion seem to be identical (at least in elastic case), this cannot be generalized to generate the confusion in the literature between “load” enhancement and “work of adhesion” enhancement, in turn apparently due to viscoelastic dissipation. Is increase of load necessarily linked to viscoelastic dissipation? Certainly this is not evident from the Irwin equation of Schapery (Eq. 4), which in the limit of very low or very fast speed gives rubbery or glassy *elastic* materials, and yet provides the enhancement.

For example, in [34] the authors study a double cantilever beam (DCB) specimen under a vertical force at constant distance from the crack tip (recalling a linearized version of the peeling problem) finding the maximum dissipation at intermediate crack propagation speed, but a monotonic increase of the load with speed. Viceversa, in the case where the distance is permitted to increase without limit, like when applying a concentrated moment to a DCB in a fixed point while the crack travels, dissipation seems to increase with load like in de Gennes’ theory [32]. In the case of indentation of a half-space by a punch, we may expect that the finite radius of the punch may play a role. Indeed, while stresses in a semi-infinite crack decay with distance from crack tip as  $r^{-1/2}$ , those far from the punch in the infinite half-space decay like  $r^{-2}$  from the resultant force hence much faster. So, although at high speed of crack propagation there must be still a “liquid” region of transition from glassy to rubbery state, this region may dissipate less than the analogous case of the semi-infinite crack. It should be mentioned that Knauss [27] tested and studied theoretically already some of the effects of finite thickness in the pure shear geometry test, and also did not find a peak in load with crack speeds, which are not really explained by the dissipation limitations at the basis of de Gennes and Persson’s finite size theories. We shall therefore investigate in details how load-enhancement varies with speed in a finite size contact, and if this is related to viscoelastic dissipation.

Recently, a few studies have been devoted to the Hertzian geometry finding complex dependences on preload and loading rate (and not only unloading rate) [35–39]. Surprisingly,

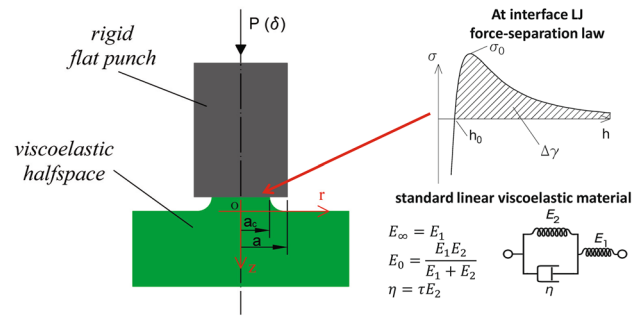


**Fig. 1** Schematic representation of the problem considered. An axisymmetric flat punch of radius  $a$  indents a linear viscoelastic half-space. A standard material is assumed with two elastic moduli  $E_0$  and  $E_\infty$  and a single relaxation time  $\tau$ . The vertical displacement of the half-space  $u_z$  and the indentation  $\delta$  are positive when the punch indents the halfspace.  $a_c$  is the radius of the ligament of the crack, and is time dependent. The punch and the substrate interact through a Lennard–Jones (LJ) force-separation law

less attention has been paid to the apparently simpler problem of the flat punch geometry, apparently also because in practise it requires special care for avoiding misalignments in an experimental setup. Here, by adopting the Boundary Element Method (BEM) we therefore explore numerically this problem with the support of extension of classical theories for the elastic case derived by Maugis [19] (see also [40]) to the viscoelastic case.

## 2 The Mechanical Model

The adhesive behaviour of an axisymmetric rigid flat punch of radius  $a$  in frictionless contact with a viscoelastic half-space is studied. For the linear viscoelastic material, the standard model is assumed, constituted by a spring placed in series with an element constituted by a dashpot and a spring in parallel (Fig. 1). The viscoelastic material has the relaxed Young’s modulus  $E_0$ , instantaneous modulus  $E_\infty$ <sup>1</sup> and the relaxation time  $\tau$ . The flat punch interacts with the viscoelastic substrate via a Lennard–Jones 3–9 force-separation law

$$\sigma(h) = \frac{8\Delta\gamma}{3h_0} \left[ \left( \frac{h_0}{h} \right)^3 - \left( \frac{h_0}{h} \right)^9 \right], \tag{7}$$

where  $\sigma$  is the traction ( $\sigma > 0$ , when tensile),  $h$  is the gap and  $h_0$  the equilibrium distance (the maximum tensile stress  $\sigma_0 = \frac{16\Delta\gamma}{9\sqrt{3}h_0}$  takes place at separation  $h = 3^1/6h_0$ ). The gap function is written as

<sup>1</sup> This notation stems from frequency dependence notation of the complex modulus  $E(\omega)$  so that  $E_0 = E(0)$  is the relaxed modulus. Other authors use the notation that  $E_0$  is the instantaneous modulus as obtained at time  $t = 0$  in a relaxation test.

$$h(r) = -\delta + h_0 + u_z(r), \tag{8}$$

where  $r$  is the radial coordinate,  $\delta > 0$  when the flat punch approaches the viscoelastic half-space,  $u_z(r)$  is the deflection of the viscoelastic half-space, which will depend on the loading history.

For elastic axisymmetric problems [18, 41]

$$u_z(r) = -\frac{1}{E^*} \int \sigma(s)G(r, s)ds, \tag{9}$$

where  $1/E^* = ((1 - \nu_1^2)/E_1 + (1 - \nu_2^2)/E_2)$  is the composite elastic modulus of the two bodies in contact,  $\sigma(s)$  is the pressure distribution (the minus sign account for the fact that we considered compressive tractions as negative),  $G(r, s)$  is the kernel function

$$G(r, s) = \begin{cases} \frac{4}{\pi r} K\left(\frac{s}{r}\right), & s < r \\ \frac{4}{\pi s} K\left(\frac{r}{s}\right), & s > r \end{cases}, \tag{10}$$

and  $K(k)$  is the complete elliptic integral of the first kind of modulus  $k$ . Hence, by using the elastic–viscoelastic correspondence principle in the form of Boltzmann integrals [42], the normal displacements of the viscoelastic half-space  $u_z(r, t)$  at time  $t$ , at location  $r$  depend on the pressure history as

$$u_z(r, t) = \frac{-1}{E_0^*} \int_{-\infty}^t \int_{-\infty}^t c(t - \tau) \frac{d\sigma(s, \tau)}{d\tau} G(r, s) s d\tau ds, \tag{11}$$

where  $c(t)$  is the dimensionless creep compliance function, which for a standard linear viscoelastic solid is

$$c(t) = E_0^* C(t) = \left[ 1 + (k - 1) \exp\left(-\frac{t}{\tau}\right) \right], \tag{12}$$

where  $k = E_0/E_\infty$ .

Equation (11), discretized in time and space, is solved to provide the adhesive solution sought. The numerical scheme is alike that in Ref. [18, 41, 44] except for accounting the viscoelastic behaviour of the half-space. The radial domain is discretized with  $N$  equally spaced elements, so that we have  $M = N + 1$  nodes where Eq. (11) is solved. From one node to the other a linear variation of the normal traction  $\sigma(s)$  is assumed, which is usually referred as “the method of the overlapping triangles” [45], and a sequential continuation algorithm is adopted in time, so that the solution  $u_z(r, t_i)$  at time  $t_i$  is used as a guess for the next time-step  $t_{i+1} = t_i + \Delta t$ , where the time increment  $\Delta t$  is kept fixed during the simulations. More details of the numerical implementation have been given in [44].

### 3 From LEFM to Uniform Debonding Behaviour

The contact of a rigid flat punch can be considered as an external crack that propagates at the interface under the action of a tensile load. If one assumes the punch to be rigid and the substrate *elastic*, neglecting friction, Maugis [19] shows

$$G = \frac{K_1^2}{2E^*} = \frac{P^2}{8\pi a^3 E^*}, \tag{13}$$

where  $G$  is the energy release rate,  $P$  is the normal load and  $K_1 = P/\sqrt{4\pi a^3}$  is the mode-I stress intensity factor. Imposing the Griffith energy balance  $G = \Delta\gamma$  [19, 46] one finds the peeling force to be

$$P = \sqrt{8\pi E^* \Delta\gamma a^3}, \tag{14}$$

where  $E^* = E/(1 - \nu^2)$ . Correspondingly the pull-off stress  $\hat{\sigma}_{po} = \max(\hat{\sigma})$  is

$$\sigma_{po} = \sqrt{\frac{8E^* \Delta\gamma}{\pi a}}, \tag{15}$$

which scales with the punch radius as  $a^{-1/2}$ , a well-known result of linear elastic fracture mechanics (LEFM). Clearly,  $\sigma_{po}$  cannot be larger than the theoretical strength of the interface  $\sigma_0$ . Hence, we define a lengthscale

$$a_0 = \frac{8E^* \Delta\gamma}{\pi \sigma_0^2}, \tag{16}$$

and only for a punch of radius  $a \gg a_0$  one expects LEFM based model to be accurate [46], while for  $a \ll a_0$  the cohesive limit is asymptotically obtained, where  $\sigma_{po} \rightarrow \sigma_0$ .

If the half-space is viscoelastic, we can consider it to behave as an elastic half-space in the limit of very slow and very fast unloading rate. In the latter case one obtains two different lengthscales  $\{a_0, a_1\}$  which refer respectively to the slow and fast unloading limits (see also Ciavarella [47] for the analogous case of “short cracks”). Recalling  $k = E_0/E_\infty < 1$ , and using  $\hat{a}_0 = a_0/h_0$  and  $\hat{\sigma}_{po} = \sigma_{po}/\sigma_0$  one gets in dimensionless form

$$\begin{cases} \hat{\sigma}_{po} = \sqrt{\frac{9\sqrt{3}}{2\pi \hat{a}_0 \Sigma_0}} < 1, \\ \hat{a}_0 = \frac{9\sqrt{3}}{2\pi \Sigma_0} \end{cases}, \quad \text{slow limit} \tag{17}$$

$$\begin{cases} \hat{\sigma}_{po} = \sqrt{\frac{9\sqrt{3}}{2\pi \hat{a}_1 \Sigma_0 k}} < 1, \\ \hat{a}_1 = \frac{9\sqrt{3}}{2\pi k \Sigma_0} \end{cases}, \quad \text{fast limit,} \tag{18}$$

where  $\Sigma_0 = \sigma_0/E_0^*$ .

### 4 Numerical Results

We conducted a wide campaign of numerical investigations, whose results are reported in this section in dimensionless form, so that the following quantities have been defined

$$\hat{a} = \frac{a}{h_0}; \quad \hat{\sigma} = \frac{\sigma}{\sigma_0}; \quad \hat{P} = \frac{P}{\pi a^2 \sigma_0};$$

$$\hat{\delta} = \frac{\delta}{h_0}; \quad \hat{t} = \frac{t}{\tau}, \tag{19}$$

while  $\hat{\sigma}_{po} = \max(\hat{\sigma})$  is the pull-off stress. Unless differently stated, we used in our simulations  $N = 200$ ,  $\Sigma_0 = 0.05$  and  $k = 0.1$ . First, let us consider the case of a punch of radius  $\hat{a}/\hat{a}_0 = 2.02$  that is unloaded from a fully relaxed viscoelastic substrate starting from  $\hat{\delta}_0 = \hat{\delta}(\hat{t}_0 = 0) = 1$  at different unloading rates  $\hat{r} = r\tau/h_0 = [0.13, 3.16, 5.01, 7.94, 12.59]$ , so that  $\hat{\delta}(\hat{t}) = \hat{\delta}_0 - \hat{r}(\hat{t} - \hat{t}_0)$ . Experimentally, this coincides with (i) indenting the viscoelastic substrate up to a prescribed indentation depth, (ii) waiting for a long dwell time so that the substrate fully relaxes, then (iii) unloading with a given (constant) displacement rate. The normalized unloading curves are shown in Fig. 2 in terms of mean normal stress versus remote indentation. As expected for a viscoelastic contact problem, the unloading rate strongly influences the unloading trajectory. For fast unloading, the substrate is stiff, hence a high load ( $K_1 \propto P$ ) is required for the crack to advance. The two linear limit behaviour on unloading in Fig. 2 correspond to instantaneous and relaxed moduli, respectively. Clearly, pull-off stress increases with rate of unloading, but the dependence is non monotonic for the work of separation per unit area  $\hat{W}_{sep} = \frac{W_{sep}}{a\sigma_0 h_0} = -\int_{\hat{\delta}_{P=0}}^{-\infty} \hat{\sigma} d\hat{\delta}$  which is proportional to the area underneath the unloading curves ( $\alpha = 9\sqrt{3}/16$ ,  $\hat{\delta}_{P=0}$  is the indentation depth when the mean stress (or the load) vanishes).

The response of a viscoelastic material is in general “history-dependent”, as from the hereditary integral in Eq. (11). Curves in Fig. 2 were obtained unloading the flat punch from a fully relaxed substrate. To investigate the effect of the loading history, we run several numerical simulations, with different loading protocols, but fixing the unloading rate at  $\hat{r} = 10$ . The simulations were conducted in displacement control and for  $\hat{\delta}(\hat{t})$  we assumed a trapezoidal function, whose key parameters are defined in the inset of Fig. 3a. We introduce the dwell time  $\hat{t}_{dwell} = \hat{t}_2 - \hat{t}_1$ , the loading rate  $\hat{r}_{load} = (\hat{\delta}_{load} - \hat{\delta}_0)/\hat{t}_1$  and the unloading rate  $\hat{r} = (\hat{\delta}_{load} - \hat{\delta}_{unload})/(\hat{t}_3 - \hat{t}_2)$ . Results in Fig. 3a and b for each unloading curve correspond to

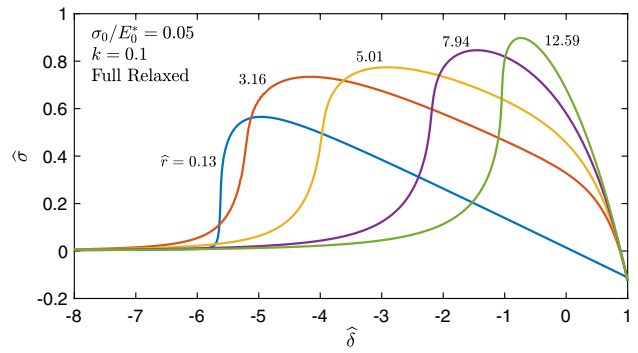


**Fig. 2** Unloading curves for  $\Sigma_0 = 0.05$ ,  $k = 0.1$ , punch of radius  $\hat{a}/\hat{a}_0 = 2.02$ , unloaded from a fully relaxed viscoelastic substrate starting from  $\hat{\delta}_0 = 1$  at different unloading rates  $\hat{r} = [0.13, 3.16, 5.01, 7.94, 12.59]$

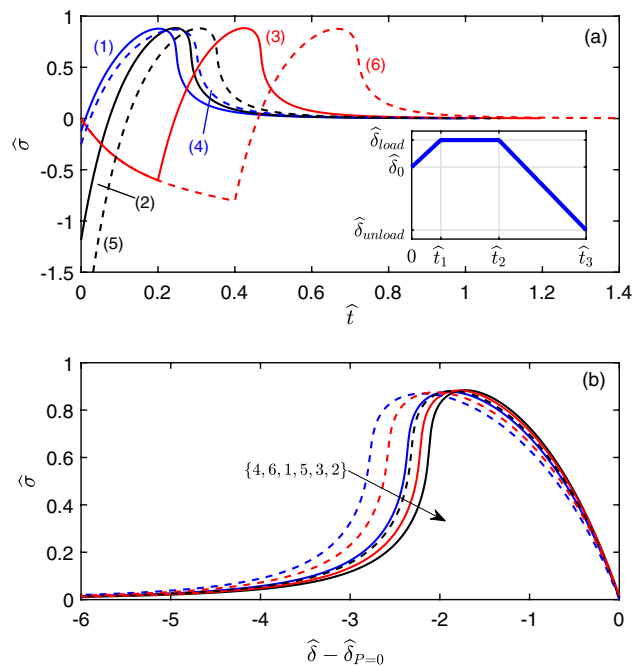


**Fig. 3 a** Unloading curves for  $\Sigma_0 = 0.05$ ,  $k = 0.1$ , punch of radius  $\hat{a}/\hat{a}_0 = 2.02$ , unloaded from a fully relaxed viscoelastic substrate starting from  $\hat{\delta}_0 = 1$  at different unloading rates  $\hat{r} = [0.13, 3.16, 5.01, 7.94, 12.59]$ . **b** The same curves shown in **a** are reported here after shifting the horizontal axis by  $\hat{\delta}_{P=0}$ , which is the indentation depth at which the normal stress vanishes during unloading

the parameters in Table 1. We considered the cases when the punch is unloaded: (i) after very slow loading from a fully relaxed substrate (blue curves, (1,4)), (ii) after very rapid loading so that the substrate appears elastic with  $E(t = 0) = E_\infty$  (black curves, (2,5)), (iii) after indenting the substrate at a constant loading rate  $\hat{r}_{load} = 5$  (red curves,

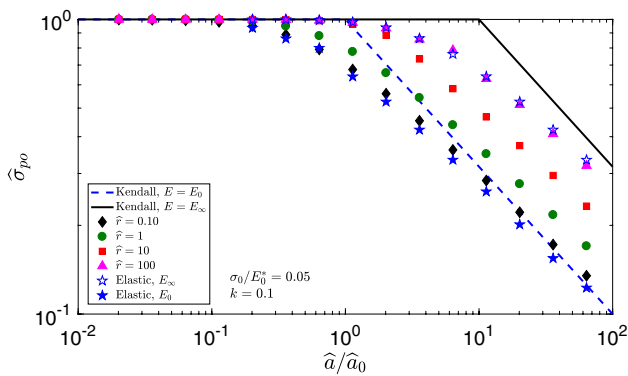


**Fig. 4** Normalized pull-off stress as a function of the normalized contact radius for  $\Sigma_0 = 0.05$ ,  $k = 0.1$ . Unloading starts from  $\hat{\delta}_0 = \hat{\delta}_{load} = 1$  from a fully relaxed substrate and is performed at a constant unloading rate  $\hat{r} = [0.1, 1, 10, 100]$ , respectively black diamonds, green circles, red squares and purple triangles. The LEFM limits for slow and fast unloading rate are shown, respectively, as blue dashed and black solid lines. Filled (empty) stars show the results obtained unloading an *elastic* substrate with  $E = E_0$  ( $E = E_\infty$ ) (Color figure online)

(3,6)). Notice that for the curves (1, 2, 4, 5) the loading phase is not shown. The maximum indentation depth  $\hat{\delta}_{load}$  was fixed equal to  $\hat{\delta}_{load} = 1$  for the curves (1, 2, 3) (solid lines) and  $\hat{\delta}_{load} = 2$  for the curves [4, 5, 6] (dashed lines). Despite the very different unloading trajectories, one notices that a key quantity such as the pull-off stress (Fig. 3a, b) is almost unaffected by the loading history. Figure 3b shows the same curves reported in Fig. 3a after shifting the horizontal axis by  $\hat{\delta}_{P=0}$ , which is the indentation depth at which the normal load vanishes during unloading, so that one can better appreciate the slight changes in the unloading trajectories. In the rest of the paper, unless differently stated, we will assume  $\hat{\delta}_0 = \hat{\delta}_{load} = 1$  and  $\hat{t}_{dwell} = 0$ .

**Table 1** Set of parameters that defines the loading protocol of the curves shown in Fig. 3a and b.

Curve	$\hat{\delta}_0$	$\hat{\delta}_{load}$	$\hat{r}_{load}$	$\hat{r}$	$\hat{t}_{dwell}$
(1) Blue solid	1	1	Very slow	10	0
(2) Black solid	1	1	Very fast	10	0
(3) Red solid	0	1	5	10	0
(4) Blue dashed	2	2	Very slow	10	0
(5) Black dashed	2	2	Very fast	10	0
(6) Red dashed	0	2	5	10	0

Notice that for all the simulations the unloading rate is fixed at  $\hat{r} = 10$  and  $\hat{t}_{dwell} = 0$  for all the simulations.

Having assessed that the loading history does not influence the pull-off stress  $\hat{\sigma}_{po}$ , in Fig. 4 we investigated the

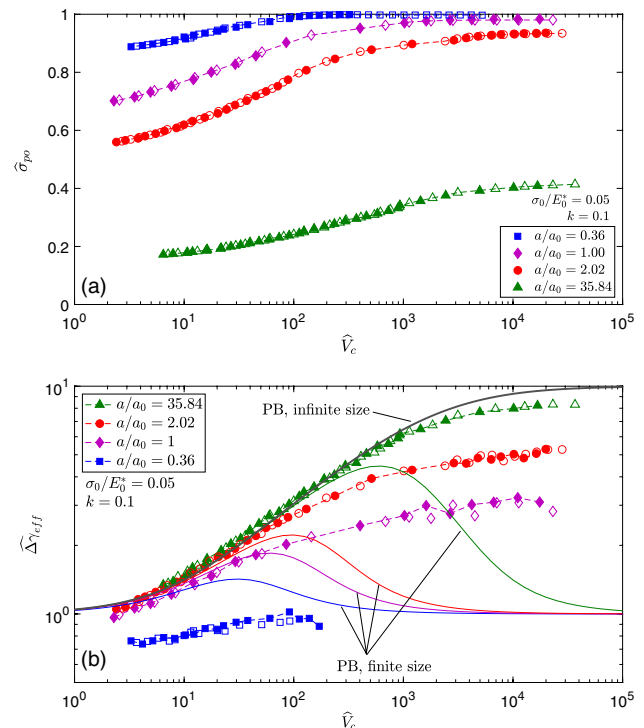


**Fig. 5** **a** Normalized pull-off stress as a function of the normalized unloading rate. **b** Normalized effective work of adhesion as a function of the crack velocity at pull-off  $\hat{v}_c$ . In **b** solid lines refer to Persson and Brener theory [29] as extended for finite size systems by Persson [43] slightly simplified by Ciavarella and Papanagelo (Eq. (17) in [31]), but with a shift on the crack velocity. The same colour corresponds to the same ratio  $\hat{a}/\hat{a}_0$ . The grey solid line refers to Persson and Brener theory for infinite systems (see Eq. (14) in Ref. [31]). In both panels  $\Sigma_0 = 0.05$ ,  $k = 0.1$ ,  $\hat{\delta}_0 = \hat{\delta}_{load} = 1$ ,  $\hat{a}/\hat{a}_0 = [0.36, 1, 2.02, 35.84]$  respectively blue squares, purple diamonds, red circles, green triangles. Filled empty symbols are used for data obtained unloading the punch form a fully relaxed substrate, while empty symbols refer to data obtained after very fast loading (Color figure online)

variation of  $\hat{\sigma}_{po}$  as a function of the normalized punch radius for four unloading rates  $\hat{r} = [0.1, 1, 10, 100]$  (respectively black diamonds, green circles, red squares and pink triangles) and starting from a fully relaxed substrate. For  $\hat{a}/\hat{a}_0 \ll 1$  the cohesive limit is reached, where the pull-off stress is independent on both the loading rate and the punch radius and it approaches the theoretical value  $\hat{\sigma}_{po} = 1$ . For  $\hat{a}/\hat{a}_0 \gg 1$  the curves follow the square root scaling imposed by LEFM, the pull-off stress increases with the unloading rate and the pull-off data remain bounded by the “slow” and “fast” limits dictated by the Kendall [46] solution (Eqs. 17, 18), respectively blue dashed and solid black lines. Notice that numerically we had to accommodate a small cohesive zone before we find the maximum force which slightly reduced the peak force from the theoretical Kendall limit (see Fig. 4).

The variation of the pull-off stress as a function of the crack speed at pull-off  $\hat{V}_c = V_c \tau / h_0$  is shown in Fig. 5a, for four different punch radii  $\hat{a}/\hat{a}_0 = [0.36, 1.00, 2.02, 35.84]$  (respectively blue, purple, red and green curves) unloading either after a very slow loading phase (filled symbols, when unloading starts  $E \simeq E_0$ ) or after a very fast loading phase (empty symbols, when unloading starts  $E \simeq E_\infty$ ) and for  $\Sigma_0 = 0.05, k = 0.1, \hat{\delta}_{load} = 1$ . As suggested in Fig. 3, the pull-off stress is not affected by the loading history, moreover for small radii (blue curve) a change of 3 orders of magnitude of the unloading rate resulted in a variation of the pull-off stress by only a 10%, as we are near the cohesive strength limit. Notice that we did not find an appreciable dependence of the pull-off stress on  $\hat{\delta}_{load}$  (not shown).

The same data shown in Fig. 5a are also reported in Fig. 5b, this time plotted as a normalized effective work of adhesion  $\hat{\Delta}\gamma_{eff} = \Delta\gamma_{eff} / \Delta\gamma$  versus the crack speed at pull-off  $\hat{V}_c$ , being  $\Delta\gamma_{eff} = P_{po}^2 / 8\pi E_0^* a_c^3$ , or, in dimensionless form  $\hat{\Delta}\gamma_{eff} = \frac{2\pi}{9\sqrt{3}} \hat{\sigma}_{po}^2 \hat{a}(\frac{\hat{a}}{\hat{a}_c})^3 \Sigma_0$ . The numerical results are compared with the prediction of Persson and Brener theory [29] as extended for finite size systems (where finite size is implied by the difference between the size of crack ligament  $a_c$  and the finite punch radius  $a$ ) by Persson [43] slightly simplified by Ciavarella and Papangelo (Eq. (17) in Ref. [31]). Notice that in order to have a reasonable agreement with the numerical results, we had to use a shift factor on the crack velocity definition<sup>2</sup> [31, 33]. The same colour corresponds to the same ratio  $\hat{a}/\hat{a}_0$ , while the grey curve is the reference to an infinite size system. The numerical results show that the effective work of adhesion increases monotonically with the crack speed in all cases. In particular, for large systems  $\hat{a}/\hat{a}_0 = 35.84$  LEFM holds, hence for slow crack velocity  $\hat{\Delta}\gamma_{eff} \simeq 1$ , while at high velocity, we obtained an enhancement close to  $E_\infty/E_0$ . For smaller radii, finite size effects come at play, but  $\hat{\Delta}\gamma_{eff}$  still increases monotonically with the crack speed. Moreover, for small radii, the normalized effective work of adhesion can be smaller than unity. This should not surprise as, even for a purely elastic problem, the pull-off stress is less than that expected from LEFM for small radii due to the transition towards the cohesive limit region which is equivalent to a reduced work of adhesion. In general, while we can say that there is a quantitative agreement with dissipation-based theories for large radii, the results contrast both quantitatively and qualitatively for finite size, and in particular, there is no evidence of a maximum of load at intermediate speeds.

<sup>2</sup> In Eq. (17) of Ref. [31] we used as a reference velocity  $v_{0,new} = 2\pi^2 v_0$ , being  $v_0 = \frac{\Delta\gamma E_0^*}{(2\pi\sigma_0)^2 \tau}$ .

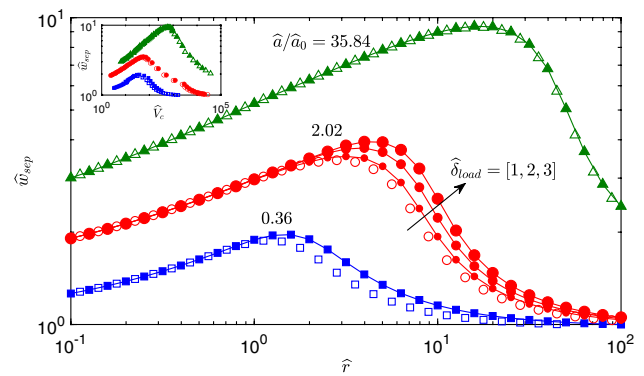


**Fig. 6** Normalized work of separation as a function of the normalized unloading rate for  $\Sigma_0 = 0.05, k = 0.1, \hat{\delta}_0 = \hat{\delta}_{load} = 1, \hat{a}/\hat{a}_0 = [0.36, 2.02, 35.84]$  respectively blue squares, red circles, green triangles. Filled symbols refer to the case when unloading starts after very slow loading, while empty symbols refer to pull-off data obtained after very fast loading. For the case  $\hat{a}/\hat{a}_0 = 2.02$  and unloading from fully relaxed substrate we tested several values of  $\hat{\delta}_0 = \hat{\delta}_{load} = [1, 2, 3]$  (the circle dimension increases with  $\hat{\delta}_{load}$ ). In the inset the work of separation is shown as a function of the crack velocity (only the data referring to  $\hat{\delta}_0 = \hat{\delta}_{load} = 1$  are shown) (Color figure online)

A key quantity to investigate is the work of separation  $\hat{w}_{sep}$ , as it gives an estimate of the energy that is dissipated during the unloading phase. We obtained this quantity as a function of the normalized unloading rate for  $\hat{\delta}_0 = \hat{\delta}_{load} = 1, \hat{a}/\hat{a}_0 = [0.36, 2.02, 35.84]$  respectively blue squares, red circles and green triangles (Fig. 6). Filled symbols refer to the case when the punch is unloaded after a very slow loading, while empty symbols refer to data obtained unloading after a very fast loading phase. The inset shows the work of separation as a function of the crack speed.

Notice that, contrary to the case of the pull-off stress and as suggested by Fig. 3, the work of separation shows a weak dependence on the loading rate, limited to small punch radius ( $\hat{a}/\hat{a}_0 = 0.36$ ) and intermediate unloading rates. For the case  $\hat{a}/\hat{a}_0 = 2.02$ , and unloading from a fully relaxed substrate, several values of  $\hat{\delta}_0 = \hat{\delta}_{load} = [1, 2, 3]$  were tested, whose results are shown as red circles with the circle dimension increasing with  $\hat{\delta}_{load}$ . For intermediate rates, we find a slight dependence of  $\hat{w}_{sep}$  on  $\hat{\delta}_{load}$ , which makes the picture a bit more elaborate than what happens for the pull-off stress. Importantly, while the pull-off stress increases monotonically with respect to the unloading rate, independently on the loading history, the work of separation retains a bell shape. Notice that for small punch radii ( $\hat{a}/\hat{a}_0 \ll 1$ ) the elastic limit at high and low velocity is  $\hat{w}_{sep} = 1$ , as we have a progressive detachment of the interface with uniform stress up to very large displacements, while in the LEFM region ( $\hat{a}/\hat{a}_0 \gg 1$ ) the elastic limit at high and low velocity is  $\hat{w}_{sep} = 2$ , because there is essentially a linear load–displacement curve up to

the “brittle” rupture at the Kendall load and it can be easily shown that the gives  $\hat{w}_{sep} = 2$ , so that some strain energy must be released at the point of fracture. Hence, the problems are in all respects elastic both at very low and very high speeds, and dissipation is not the cause of the load enhancement at fast unloading, contrary to the classical de Gennes picture. The load increases of the ratio instantaneous to relaxed moduli, but the remote displacement decreases by the same ratio, hence the resulting area integral is the same at very low unloading rates, and at very high ones.

### 5 Extension of Maugis Cohesive Zone Model

In this section, we attempt a generalization of the elastic cohesive model of Maugis [19] (see also the work of Tang and Hui [40]) to the case of viscoelasticity. The problem of unloading a rigid axisymmetric flat punch from an elastic half-space of composite elastic modulus  $E^*$  has been studied using a Dugdale cohesive law [19, 40] which showed that the peeling force  $P$  is related to the radius of the ligament of the crack  $a_c$  as follows

$$P = 2a_c \sigma_0 \left[ \sqrt{a^2 - a_c^2} + \frac{a^2}{a_c} \cos^{-1} \frac{a_c}{a} \right], \tag{20}$$

where we recall  $a$  is the punch radius, while  $a_c$  is the radius of the ligament of the crack which is a function of time, hence the cohesive stresses may exist in the annulus  $a_c \leq r \leq a$ . The pull-off occurs when the separation at the crack mouth  $r = a$  reaches the Critical Opening Distance (COD)  $h_c$  in the Dugdale force-separation law, as any smaller radius would lead to a smaller force. Considering the crack profile this condition translates into [40]

$$h_c = \frac{4\sigma_0}{\pi E^*} \left[ a_c - a + \sqrt{a^2 - a_c^2} \cos^{-1} \frac{a_c}{a} \right], \tag{21}$$

where equating the surface energy  $\Delta\gamma$  in a LJ force-separation law with that of a Dugdale model and having the same theoretical strength  $\sigma_0$ , gives  $h_c = ah_0 \simeq 0.974h_0$ . Solving Eq. (21) for  $a_c$  one determines the critical radius of the ligament of the crack at pull-off and substituting into Eq. (20) the pull-off force is obtained. In the dimensionless formulation introduced before the equation for the normal stress is unaffected by the modulus

$$\hat{\sigma} = \frac{2}{\pi} \frac{\hat{a}_c}{\hat{a}} \left[ \sqrt{1 - \left(\frac{\hat{a}_c}{\hat{a}}\right)^2} + \frac{\hat{a}_c}{\hat{a}} \cos^{-1} \frac{\hat{a}_c}{\hat{a}} \right], \tag{22}$$

while the condition for the COD is modified for a viscoelastic half-space, by substituting the inverse of the elastic

modulus with an effective compliance  $c_{eff}(\hat{t}_b) = E_0^* C(t_b)$ , with  $t_b$  a characteristic time

$$\frac{4\Sigma_0}{\pi} c_{eff}(\hat{t}_b) \left[ \hat{a}_c - \hat{a} + \hat{a} \sqrt{1 - \left(\frac{\hat{a}_c}{\hat{a}}\right)^2} \cos^{-1} \frac{\hat{a}_c}{\hat{a}} \right] - \frac{9\sqrt{3}}{16} = 0. \tag{23}$$

In analogy with the suggestion of Schapery, we define  $t_b \simeq b/V$  being  $b$  the width of the cohesive zone and  $V$  the crack velocity.<sup>3</sup> For semi-infinite crack, and a Dugdale cohesive stress law, Schapery found

$$b = \frac{\pi}{8} \left( \frac{K_I}{\sigma_0} \right)^2 = \frac{\pi^2}{32} \left( \frac{\sigma}{\sigma_0} \right)^2 \left( \frac{a}{a_c} \right)^4 a_c, \tag{24}$$

where we assumed, during propagation, the mode-I SIF is given by  $K_I = P/\sqrt{4\pi a_c^3}$ . In the numerical simulation, we used a standard linear viscoelastic material, hence

$$c_{eff}(\hat{t}_b) = 1 + (k - 1) \exp \left[ -\frac{\pi^2}{96} \frac{\hat{\sigma}^2 \hat{a}_c}{\hat{V}} \left( \frac{\hat{a}}{\hat{a}_c} \right)^4 \right]. \tag{25}$$

At every time-step we determined the crack position based on the location of the maximum adhesive stress at the interface, hence we estimated  $V_c$ , the crack velocity at pull-off, and used this value in the Cohesive Zone Model (CZM, Eqs. 25, 23, 22) to determine the theoretical pull-off stress which was then compared with that obtained numerically in Fig. 7 for a set of punch radii  $\hat{a}/\hat{a}_0 = [0.36, 2.02, 3.58, 35.84]$  (respectively blue squares, red circles, black stars, green triangles) unloading from a fully relaxed substrate (filled symbols,  $E \simeq E_0$  when unloading starts) or from a not-relaxed substrate (empty symbols,  $E \simeq E_\infty$  when unloading starts). Although small discrepancies appear with respect to the numerical data, the CZM provides a fairly good estimate of the pull-off stress, with deviations not larger than a 10% between numerical and theoretical data.

As with semi-infinite crack theories, we have described the model as a function of the crack speed, which, in an adhesive experiment, is unlikely to be constant and has to be measured in numerical/real experiments, where generally the remote displacement rate is imposed. The relation between the external unloading rate  $\hat{r}$  with the crack speed at pull-off  $\hat{V}_c$  is shown in Fig. 8 for the same data as in Fig. 7. For small punch radii (blue squares) the behaviour is almost linear and a small deviation can be seen only around  $\hat{r} \approx 2$ , while for  $\hat{a}/\hat{a}_0 > 1$  we clearly found two linear regimes and

<sup>3</sup> Schapery uses  $t_b = b/3V$ , for a constant stress (Dugdale) model.



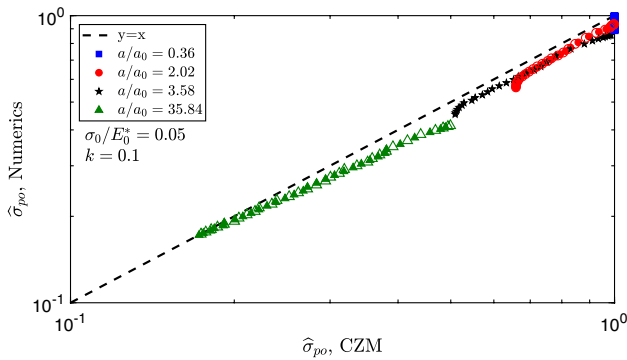


**Fig. 7** The pull-off stress obtained with BEM numerical simulations is compared with that predicted by the CZM (Eqs. 22, 23, 25) for the following set of parameters  $\Sigma_0 = 0.05$ ,  $k = 0.1$ ,  $\hat{\delta}_0 = \hat{\delta}_{load} = 1$  and  $\hat{a}/\hat{a}_0 = [0.36, 2.02, 3.58, 35.84]$ , respectively blue squares, red circles, black stars, green triangles. Filled (Empty) symbols refer to the case when unloading starts from a relaxed (unrelaxed) substrate (Color figure online)

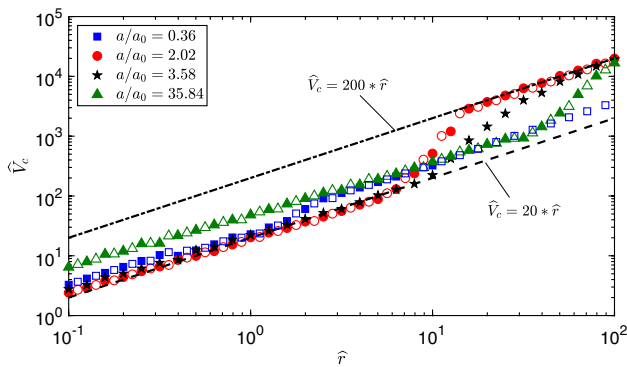


**Fig. 8** Crack propagation velocity at pull-off  $\hat{V}_c$  as a function of the unloading rate  $\hat{r}$  for the same data as in Fig. 7, (the same symbols are used)

a transition zone between the two linear dashed lines shown in Fig. 8, which perhaps may be used to roughly estimate the crack speed as a function of the loading rate.

## 6 Conclusions

In this work, we have studied the adhesive behaviour of a circular rigid flat punch that is placed in contact with a viscoelastic half-space. We showed that depending on the punch radius there exists a transition from a cohesive limit, where debonding happens at a uniform stress equal to the theoretical strength of the interface, to a regime that is governed by classical LFM concepts, extended to the viscoelastic case. Our study has focussed on two key quantities, such as the pull-off stress and the work of separation. We found that the pull-off stress is a monotonically

increasing quantity of the unloading rate and is almost independent on the contact history. This is markedly different from the case of a Hertzian indenter which has been extensively studied [36–38] and showed a strong influence on the preload. Indeed, we suggest here that the dependence on the loading history of the pull-off stress is geometry dependent. In our numerical simulations we also measured the work of separation  $w_{sep}$  as the energy per unit area that is dissipated to separate the contact. Indeed, in an attempt to interpret the maximum of load (and resulting instability) in the peeling experiments of Gent and Petrich [16], de Gennes [28] proposed a theory of viscoelastic semi-infinite crack propagation based on *dissipation* away from the crack tip reaching a maximum at intermediate speeds. We found that  $w_{sep}$  has indeed a maximum at intermediate crack speed, but this does not correspond to a maximum of the load and hence dissipated energy cannot be directly used to determine the debonding load. Notice that in our geometry, where the flat punch is rigid, the stress intensity factor  $K_I$  doesn't need any geometrical correction factor as for example introduced in [48] as it is always equal to  $K_I = P/\sqrt{4\pi a_c^3}$  where  $a_c$  is initially the punch radius but then becomes the current size of the ligament of the crack. Hence our numerical results cannot be explained by a “corrected” Persson–Brener theory for infinite systems as suggested by Violano et al. [48] for a finite viscoelastic plate geometry. Finally, we have proposed a cohesive zone model for debonding of a flat punch from a viscoelastic substrate, stemming from the elastic theory by Maugis [19] (see also [40]), which proved to be reasonably good in terms of pull-off stress prediction. Unfortunately, in general we cannot impose externally the crack speed, but the remote displacement rate, and hence the theory only interprets data but is not predictive.

**Author Contributions** A.P. and M.C. contributed equally to this work.

**Funding** Open access funding provided by Politecnico di Bari within the CRUI-CARE Agreement. A.P. was supported by the European Union (ERC-2021-STG, “Towards Future Interfaces With Tuneable Adhesion By Dynamic Excitation” - SURFACE, Project ID: 101039198, CUP: D95F22000430006). Views and opinions expressed are however those of the authors only and do not necessarily reflect those of the European Union or the European Research Council. Neither the European Union nor the granting authority can be held responsible for them. A.P. was partially supported by Regione Puglia (Italy), project ENOVIM (CUP: D95F21000910002) granted within the call “Progetti di ricerca scientifica innovativi di elevato standard internazionale” (art. 22 della legge regionale 30 novembre 2019, n. 52 approvata con A.D. n. 89 of 10-02-2021, BURP n. 25 del 18-02-2021). A.P. and M.C. acknowledge support by the Italian Ministry of University and Research (MUR) under the programme “Department of Excellence” Legge 232/2016 (Grant No. CUP—D93C23000100001).

**Data Availability** The dataset generated for this article is available at <https://doi.org/10.5281/zenodo.7757174>.

## Declarations

**Conflicts of interest** The authors have no relevant financial or non-financial interests to disclose.

**Open Access** This article is licensed under a Creative Commons Attribution 4.0 International License, which permits use, sharing, adaptation, distribution and reproduction in any medium or format, as long as you give appropriate credit to the original author(s) and the source, provide a link to the Creative Commons licence, and indicate if changes were made. The images or other third party material in this article are included in the article's Creative Commons licence, unless indicated otherwise in a credit line to the material. If material is not included in the article's Creative Commons licence and your intended use is not permitted by statutory regulation or exceeds the permitted use, you will need to obtain permission directly from the copyright holder. To view a copy of this licence, visit <http://creativecommons.org/licenses/by/4.0/>.

## References

- Giordano, G., Carloti, M., Mazzolai, B.: A perspective on cephalopods mimicry and bioinspired technologies toward proprioceptive autonomous soft robots. *Adv. Mater. Technol.* **6**(12), 2100437 (2021)
- Mazzolai, B., Mondini, A., Tramacere, F., Riccomi, G., Sadeghi, A., Giordano, G., Carminati, S.: Octopus-inspired soft arm with suction cups for enhanced grasping tasks in confined environments. *Adv. Intell. Syst.* **1**(6), 1900041 (2019)
- Giordano, G., Gagliardi, M., Huan, Y., Carloti, M., Mariani, A., Menciaci, A., Sinibaldi, E., Mazzolai, B.: Toward mechanochromic soft material-based visual feedback for electronics-free surgical effectors. *Adv. Sci.* **8**(15), 2100418 (2021)
- Cacucciolo, V., Shintake, J., Kuwajima, Y., Maeda, S., Floreano, D., Shea, H.: Stretchable pumps for soft machines. *Nature* **572**(7770), 516–519 (2019)
- Shui, L., Jia, L., Li, H., Guo, J., Guo, Z., Liu, Y., Chen, X.: Rapid and continuous regulating adhesion strength by mechanical microvibration. *Nat. Commun.* **11**(1), 1–7 (2020)
- Arzt, E., Quan, H., McMeeking, R.M., Hensel, R.: Functional surface microstructures inspired by nature—from adhesion and wetting principles to sustainable new devices. *Prog. Mater. Sci.* **120**, 100778 (2021)
- Lunni, D., Giordano, G., Pignatelli, F., Filippeschi, C., Linari, S., Sinibaldi, E., Mazzolai, B.: Light-assisted electrospinning monitoring for soft polymeric nanofibers. *Sci. Rep.* **10**(1), 1–12 (2020)
- Lunni, D., Giordano, G., Sinibaldi, E., Cianchetti, M., Mazzolai, B.: Shape estimation based on kalman filtering: Towards fully soft proprioception. In 2018 IEEE International Conference on Soft Robotics (RoboSoft). IEEE, pp. 541–546 (2018)
- Asbeck, A., Dastoor, S., Parness, A., Fullerton, L., Esparza, N., Soto, D., et al.: Climbing rough vertical surfaces with hierarchical directional adhesion. In 2009 IEEE International Conference on Robotics and Automation. IEEE, pp. 2675–2680 (2009)
- Shintake, J., Cacucciolo, V., Floreano, D., Shea, H.: Soft robotic grippers. *Adv. Mater.* **30**(29), 1707035 (2018)
- Dahlquist, C.A.: Pressure-sensitive adhesives. In: Patrick, R.L. (ed.) *Treatise on Adhesion and Adhesives*, vol. 2, pp. 219–260. Dekker, New York (1969)
- Creton, C., Ciccotti, M.: Fracture and adhesion of soft materials: a review. *Rep. Prog. Phys.* **79**(4), 046601 (2016)
- Ciavarella, M., Papangelo, A., McMeeking, R.: Crack propagation at the interface between viscoelastic and elastic materials. *Eng. Fract. Mech.* **257**, 108009 (2021)
- Barquins, M., Maugis, D.: Tackiness of elastomers. *J. Adhes.* **13**(1), 53–65 (1981)
- Gent, A.N., Schultz, J.: Effect of wetting liquids on the strength of adhesion of viscoelastic material. *J. Adhes.* **3**(4), 281–294 (1972)
- Gent, A.N., Petrich, R.P.: Adhesion of viscoelastic materials to rigid substrates. *Proc. R. Soc. Lond. A Math. Phys. Sci.* **310**(1502), 433–448 (1969)
- Andrews, E.H., Kinloch, A.J.: Mechanics of elastomeric adhesion. *J. Polym. Sci.* **46**(1), 1–14 (1974)
- Greenwood, J.A., Johnson, K.L.: The mechanics of adhesion of viscoelastic solids. *Philos. Mag. A* **43**, 697–711 (1981)
- Maugis, D.: Adhesion of spheres: the JKR-DMT transition using a Dugdale model. *J. Colloid Interface Sci.* **150**(1), 243–269 (1992)
- Rivlin, R.: *The Effective Work of Adhesion*, p. 215. Springer, New York (1997)
- Williams, M.L., Landel, R.F., Ferry, J.D.: The temperature dependence of relaxation mechanisms in amorphous polymers and other glass-forming liquids. *J. Am. Chem. Soc.* **77**, 3701–3707 (1955)
- Ceglie, M., Menga, N., Carbone, G.: The role of interfacial friction on the peeling of thin viscoelastic tapes. *J. Mech. Phys. Solids* **159**, 104706 (2022)
- Rice, J.R.: *Mechanics of Quasi-static Crack Growth* (No. COO-3084-63; CONF-780608-3). Brown University, Providence (1978)
- Graham, G.A.C.: Two extending crack problems in linear viscoelasticity theory. *Q. Appl. Math.* **27**, 497–507 (1969)
- Schapery, R.A.: A theory of crack initiation and growth in viscoelastic media. *Int. J. Fracture* **11**, 141–159 (1975)
- Schapery, R.A.: A theory of crack initiation and growth in viscoelastic media II. Approximate methods of analysis. *Int. J. Fracture* **11**(3), 369–388 (1975)
- Knauss, W.G.: On the steady propagation of a crack in a viscoelastic sheet: experiments and analysis. In: Kausch HH, Hassel IA, Jaffe RE (eds) *Deformation and fracture of high polymers*. In: *Proceedings of the Same-name 1972 Conference in Kronberg, Germany*. Plenum Press, New York, pp. 501–541 (1973)
- de Gennes, P.G.: Soft adhesives. *Langmuir* **12**(19), 4497–4500 (1996)
- Persson, B.N.J., Brener, E.A.: Crack propagation in viscoelastic solids. *Phys. Rev. E* **71**(3), 036123 (2005)
- Hui, C.Y., Zhu, B., Long, R.: Steady state crack growth in viscoelastic solids: a comparative study. *J. Mech. Phys. Solids* **159**, 104748 (2022)
- Ciavarella, M., Papangelo, A.: Effects of finite thickness on crack propagation in viscoelastic materials. *Eng. Fract. Mech.* **248**, 107703 (2021)
- Ciavarella, M., Papangelo, A., McMeeking, R.: On transient and steady state viscoelastic crack propagation in a double cantilever beam specimen. *Int. J. Mech. Sci.* **229**, 107510 (2022). <https://doi.org/10.1016/j.ijmecsci.2022.107510>
- Ciavarella, M., Cricri, G., McMeeking, R.: A comparison of crack propagation theories in viscoelastic materials. *Theoret. Appl. Fract. Mech.* **116**, 103113 (2021)
- Xu, D.B., Hui, C.Y., Kramer, E.J.: Interface fracture and viscoelastic deformation in finite size specimens. *J. Appl. Phys.* **72**(8), 3305–3316 (1992)
- Ciavarella, M.: An upper bound for viscoelastic pull-off of a sphere with a Maugis–Dugdale model. *J. Adhes.* **98**, 1–14 (2021)
- Afferrante, L., Violano, G.: On the effective surface energy in viscoelastic Hertzian contacts. *J. Mech. Phys. Solids* **158**, 104669 (2022)
- Violano, G., Afferrante, L.: Size effects in adhesive contacts of viscoelastic media. *Eur. J. Mech. A Solids* **96**, 104665 (2022)
- Violano, G., Afferrante, L.: On the long and short-range adhesive interactions in viscoelastic contacts. *Tribol. Lett.* **70**(3), 1–5 (2022)

39. Müser, M.H., Persson, B.N.: Crack and pull-off dynamics of adhesive, viscoelastic solids. *Europhys. Lett.* **137**(3), 36004 (2022)
40. Tang, T., Hui, C.Y.: Decohesion of a rigid punch from an elastic layer: transition from “flaw sensitive” to “flaw insensitive” regime. *J. Polym. Sci. B Polym. Phys.* **43**(24), 3628–3637 (2005)
41. Feng, J.Q.: Contact behavior of spherical elastic particles: a computational study of particle adhesion and deformations. *Colloids Surf. A* **172**(1–3), 175–198 (2000)
42. Christensen, R.: *Theory of Viscoelasticity: An Introduction*. Elsevier, Berlin (2012)
43. Persson, B.N.J.: Crack propagation in finite-sized viscoelastic solids with application to adhesion. *Europhys. Lett.* **119**(1), 18002 (2017)
44. Papangelo, A., Ciavarella, M.: A numerical study on roughness-induced adhesion enhancement in a sphere with an axisymmetric sinusoidal waviness using Lennard-Jones interaction law. *Lubricants* **8**(9), 90 (2020)
45. Johnson, K.L.: *Contact Mechanics*. Cambridge University Press, Cambridge (1987)
46. Kendall, K.: The adhesion and surface energy of elastic solids. *J. Phys. D Appl. Phys.* **4**(8), 1186 (1971)
47. Ciavarella, M.: Viscoelastic short cracks propagation. *Eng. Fract. Mech.* **264**, 108276 (2022)
48. Violano, G., De Carolis, S., Palmieri, M.E., Carbone, G., Tricarico, L., Demelio, G.P., Afferrante, L.: Crack propagation in viscoelastic finite-sized solids: theory and experiments. *IOP Conf. Ser. Mater. Sci. Eng.* **1275**, 012043 (2023)

**Publisher's Note** Springer Nature remains neutral with regard to jurisdictional claims in published maps and institutional affiliations.